Tanzania Journal of Engineering and Technology 2025, **44(1)**:1-17
OPEN ACCESS articles distributed under Creative Commons Attribution
Licence [CC BY-ND]
Websites: https://ajol.org/tjet; https://tjet.udsm.ac.tz

ISSN 1821-536X (**print**); ISSN 2619-8789 (**electronic**)
https://doi.org/10.52339/tjet.v44i1.987

Regular Research Manuscript

Influence of Substrate Temperature on the Properties of Reactive DC Magnetron Co-Sputtered Ag-doped TiO_2 Thin Films

Hezekiah B. Sawa†, Margaret E. Samiji and Nuru R. Mlyuka

Physics Department, University of Dar es Salaam, P. O. Box 35063, Dar es Salaam, Tanzania

†Corresponding author: sawa.hezekiah@udsm.ac.tz; ORCID: 0000-0002-7846-5575

ABSTRACT

This study reports on the influence of substrate temperature on the properties of Ag-doped TiO_2 thin films. The films were deposited by reactive DC co-sputtering of Ti and Ag targets at different substrate temperatures and Ag target sputtering powers. Grazing incident X-ray diffractometer confirmed that all films were polycrystalline with dominant peak oriented along (101) planes representing the anatase TiO_2 phase. The average grain size of the samples improved with increase in deposition temperature. At a substrate temperature of 450 ℃, the samples had a dominant peak representing the rutile phase, suggesting partial transformation from anatase to rutile phase. The electrical conductivity of the samples increased with increase in substrate temperature; however, the average solar transmittance was decreased. Ag doping increased the electrical conductivity of the TiO_2 samples by one order of magnitude compared to the undoped ones. A good compromise between the electrical conductivity (1.304 $(\Omega cm)^{-1}$) and solar transmittance (> 62%) was obtained at a substrate temperature of 400 ℃ and Ag dopant concentrations of 0.2% and 0.28% as determined by Rutherford Backscattering measurements. These results demonstrate the potential of Ag doping and optimisation of deposition conditions for the realisation of TiO_2 based transparent conducting oxide that meets requirements for practical applications in optoelectronic devices. However, investigation of the effects of Ag-doped TiO_2 transparent contact on the performance of these devices, particularly thin film solar cells, is important. This can also include gaining insight on the quality of the interface between Ag-doped TiO_2 transparent contact and solar cells' layers and hence device performance.

ARTICLE INFO

Submitted: Mar. 12, 2024

Revised: Oct. 25, 2024

Accepted: Jan. 12, 2025

Published: Apr. 2025

Keywords: *Substrate temperature, Ag doping, Ag-doped TiO_2, TiO_2, reactive co-sputtering.*

INTRODUCTION

Transparent conductive oxides (TCOs) are characterized by simultaneous high electrical conductivity and optical transmittance. These materials are widely used in optoelectronic devices such as photovoltaic cells, optical waveguides, light emitting and laser diodes and sensors (Shao, 2024; Sawa *et al.*, 2024 (a); Mwakyusa *et al.*, 2022; Ellmer, 2012; Granqvist, 2007) Among the materials, tin-doped indium oxide (ITO) is the most established, widely used and dominating TCO in the market (Ollotu *et al.*, 2020;

Platzer-Björkman *et al*., 2019; Ellmer, 2012). However, ITO scalability is limited by the high cost of indium which consequently triggers significant research efforts toward finding alternative materials (Sawa *et al*., 2024(b); Green, 2009). Low cost, earth-abundant and environmentally friendly wide bandgap TiO_2 is one of the promising alternatives to ITO for most of the applications (Ifeoma and Jude, 2018). Due to its potential, TiO_2 has been extensively used in several applications including as an antireflection coating (Zhang *et al*., 2021; Mlyuka *et al*., 2009), gas sensing (Sheini and Rohani, 2016) and as an electron transport layer in perovskite based solar cells (Tavakoli *et al*., 2018). Additionally, it has been investigated as a buffer layer in thin film solar cells such as kesterite-based solar cells (Nisika *et al*., 2021; Chihi *et al*., 2017). Despite its wide use, making TiO_2 with high conductivity and transmittance simultaneously is still a challenge. The low conductivity in TiO_2 is mainly attributed to the carrier recombination due to its deep trapping centres (Chakhtouna *et al*., 2021). Among the approaches that have the potential to improve both transmittance and conductivity are incorporating dopants and controlling deposition conditions (Liaqat *et al*., 2020; Yin *et al*., 2017). Furthermore, dopants with controlled amounts can not only improve conductivity and transmittance but also enhance other properties such as morphologies and crystal structures (Roose *et al*., 2015).

Several metals such as Zr, Nb, Zn, In and Ag among others, have been investigated as dopants for TiO_2 TCO (Chakhtouna *et al*., 2021; Panigrahi and Devi, 2019; Yin *et al*., 2017; Peng *et al*., 2016;Wu *et al*., 2016; Zhang *et al*., 2016). Amongst these, Ag is one of the most promising due to favourable properties such as comparable atomic radii (0.144 nm for Ag and 0.147 nm for Ti) for substituting Ti host atoms in the TiO_2 lattice. The comparable atomic sizes help to avoid or reduce lattice defects due to atomic mismatching in the TiO_2 structure. It has been reported that Ag dopant reduces the recombination of the photo-generated charge carriers in TiO_2 (Chakhtouna et al., 2021; Naghdi et al., 2018), resulting in improved electrical conductivity without compromising transmittance.

Several methods for depositing Ag-doped TiO_2 TCO have been reported. These include electron beam evaporation (Lu et al., 2011), spin coating (Liaqat et al., 2020), field-assisted spray pyrolysis (Ifeoma and Jude, 2018), and sputtering (Agirseven *et al*., 2020). Sputtering is one of the simple, cheap and well-established methods of which uniformly compacted films can be reproduced and the level of dopant concentration can easily be controlled (Shana *et al*., 2023). Under this method, doping can be done through two approaches; one is sputtering of the industrially doped target (Ag:TiO or Ag:Ti). This approach requires the concentration of dopant in the parent target to be predetermined, and hence to optimise doping levels in the prepared TiO_2 films many sputtering targets with different dopant concentrations are needed. The other approach is doping by co-sputtering (Agirseven *et al*., 2020) of the host Ti metal and dopant targets under a controlled oxygen to argon gas ratio. In this method, doping levels can be controlled by adjusting the sputtering powers to each target. This approach is more advantageous over the previous one as it provides freedom to optimise doping levels and requires only two targets.

Sputtering conditions that influence properties of TiO_2 films include sputtering pressure, oxygen to argon partial pressure and substrate temperature (Ananthakumar *et al*., 2012). Substrate temperature affects the oxidation process, mobility and hence kinetic energy of the incident species that determine condensation, crystal growth and nucleation of adatoms on the substrate (Das et al., 2020, Mlyuka and Kivaisi, 2006). As a result, substrate temperature significantly influences both the electrical conductivity and transmittance of the films. There are several studies on Ag-doped TiO_2 films (Al-Maliki *et al*., 2020; Liaqat *et al*., 2020; Soylu *et al*., 2019; Lei *et al*., 2014), but yet the influence of substrate temperature and optimised Ag doping through reactive magnetron DC co-sputtering on the properties of the Ag-doped TiO_2 films are not fully elucidated. Thus, this work reports on the influence of deposition substrate temperature and Ag doping on the structural, morphological, optical and electrical properties of Ag-doped TiO_2 thin films deposited by reactive co-sputtering of Ti and Ag targets at controlled argon and oxygen gas environment.

MATERIALS AND METHODS

Ultrasonically cleaned soda lime glass (SLG) substrates were used for the deposition of the TiO_2 and Ag-doped TiO_2 TCOs by DC magnetron sputtering method. During cleaning, SLG substrates were placed in a warm soap solution for 15 min; thereafter the substrates were washed and then rinsed with distilled water and ethanol as described in our previous work (Sawa *et al*., 2018). Substrates were later placed in an ultrasonic bath (Decon FS3000 frequency sweeper) containing distilled water for 25 min and then dried in ethanol vapour. The cleaned substrates were stored in the desiccator containing silica gels to keep them dry and free from contamination.

TiO_2 and Ag-doped TiO_2 films were deposited by reactive DC co-sputtering of Ti and Ag metallic targets with 99.995% purities with the system base pressure of ~ 1 x 10^{-5} mbar. Further details on the set-up of the sputtering system can be found in the work by Haji *et al*. (2023). Before the substrate temperature was varied, sputtering powers for Ag and Ti targets, O_2 and Ar flow rates were optimised while the substrate temperature was set at 300 °C. Sputtering powers of 0.2 W, 0.5 W and 0.8 W were used for the Ag target while that for Ti target was set at 150 W. O_2 and Ar flow rates were set at 2.5 sccm and 50 sccm, respectively through mass flow gas controller (Bronkhost High-tech, E-5752-AAA) resulting into a working pressure of 5.7 x 10^{-3} mbar. For the optimal Ag target sputtering power of 0.5 W, Ar and O_2 flow rates, Ti target sputtering power and substrate temperature were systematically varied in order to optimise the films transmittance and Hall effects parameters. At the optimised substrate temperature, Ag sputtering power was varied from 0. 2 W to 1.5 W.

The KLA Tencor Alpha Step IQ Surface Profiler was used to measure the films thickness. The spectral transmittance of the films was measured by using the Perkin Elmer Lambda 1050+ UV/VIS/NIR spectrometer and the Hall effect parameters were determined by using the Ecopia HMS 3000, 5.7 T Hall Effect Measurement System. Glow Discharge Optical Emission Spectroscopy (GDOES) with a Spectruma Analytic GDA750HR analyser using Ar as the sputtering gas and a probe diameter of 2 mm was used to study depth composition profiles of Ag, Ti and O elements. Rutherford Backscattering (RBS) analysis was performed to determine the Ag dopants' concentration in the films. The structural properties of the films were studied using Grazing Incidence X- Ray Diffractometer (GIXRD) at Kα1 radiation with a wavelength of 0.154056 nm and a grazing incidence angle of 1° in parallel beam geometry. Raman spectroscopy was used to confirm the crystal structure. The morphology of the samples was determined using Field Emission Scanning Electron Microscopy (FE-SEM). The measurements were carried out at 2 kV and a magnification of 75 K ×. A Veeco Instrument, Nanoscope IIIA Atomic Force Microscopy (AFM) with RTESP7 and a 125 μm pyramidal silicon tip was used to study the surface morphology. 1 μm x 1 μm images of the films were scanned at a rate of 2 Hz and the images were then analysed using Gwydion and WSxM software, as described by Nečas and Klapetek *et al.*

(2012) and Horcas *et al.* (2007), respectively.

RESULTS AND DISCUSSION

Optimisation of Sputtering Powers and Gas Flow Rates at Low Substrate Temperature

Both the electrical conductivity and optical transmittance of the Ag-doped TiO_2 thin films depend on the substrate temperature and other sputtering conditions. In this study, before investigating the influence of substrate temperature, sputtering powers (for both Ti and Ag targets) and gas flow rates of O_2 and Ar were optimised to improve the transmittance and lower the sheet resistance of the films.

Initially, Ag-doped TiO_2 samples with different Ag concentrations were prepared by varying the sputtering power to the Ag target while keeping other conditions constant. It was found that the Ag-doped films had a lower sheet resistance than the un-doped samples (180 kΩ per square). The doped films at 0.5 W Ag target sputtering power had the lowest sheet resistance, less than 50 kΩ per square compared to 90 kΩ/square and 58 kΩ/square for the samples doped with Ag at 0. 2 W and 0.8 W Ag target sputtering powers, respectively. On the other hand, samples doped at 0.2 W had transmittance (both in the visible and near-infrared region) comparable to that of undoped films but significantly higher than the transmittance of films doped at higher sputtering powers as shown in Figure 1. When both the optical transmittance and sheet resistance were taken into consideration, it was found that samples doped at 0.5 W were having low sheet resistance and transmittance comparable to that of undoped films**.**

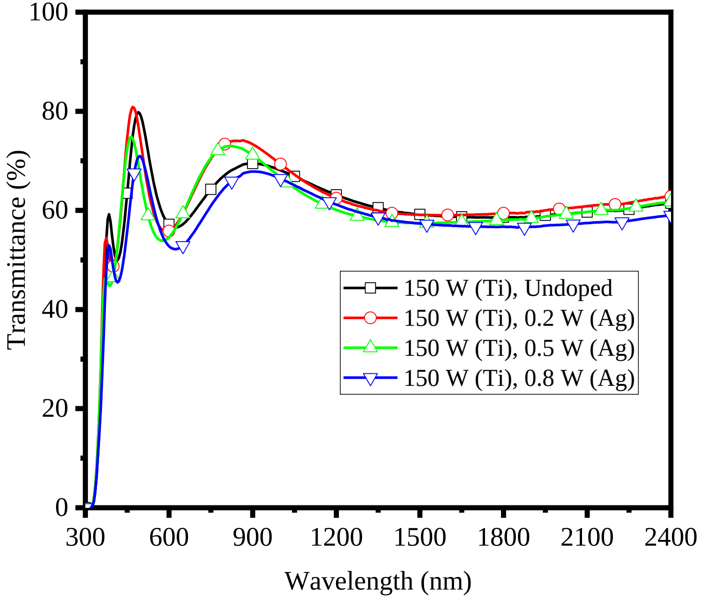

Figure 1: Transmittance of Ag-doped TiO_2 films deposited at 300 °C with different Ag target sputtering powers.

In the subsequent samples' preparation, the sputtering power of the Ag target was fixed at 0.5 W while the Ar flow rate was set at different values of 50 sccm, 60 sccm and 40 sccm. The sheet resistance of the samples deposited at 60 sccm and 50 sccm Ar flow rates were found to be approximately 25 kΩ per square and 50 kΩ per square, respectively, whereas samples deposited at 40 sccm were non-conductive. Transmittance of the samples deposited at 60 sccm was low, although they had lower sheet resistance while samples deposited at 40 sccm showed improved transmittance as shown in Figure 2. Consequently, Ar flow rate of 50 sccm was selected for the subsequent O_2 flow rate and Ti target sputtering power optimisation for the Ag-doped TiO_2 depositions. In the subsequent sample preparations, the O_2 flow rate was changed from 2.5 sccm to 3.0 sccm at a fixed Ar flow rate of 50 sccm. At 3.0 sccm of O_2, both transmittance and sheet resistance of the samples were found to be higher compared to those for samples deposited at lower flow rates. In an attempt to achieve even higher transmittance and lower sheet resistance, Ti target sputtering power was varied at 150 W, 180 W and 200 W, while other deposition conditions were kept constant. The spectral transmittance of the films was found to decrease with increase of the Ti target sputtering power as shown in Figure 2. The slightly improved transmittance and reduced sheet resistance were found at sputtering powers of 180 W and 0.5 W for Ti and Ag targets, respectively, while Ar and O_2 flow rates were set at 50 sccm and 3.0 sccm, respectively. These optimal sputtering conditions were then used in samples deposition to study the effects of substrate temperature on the properties of Ag-doped TiO_2 thin films.

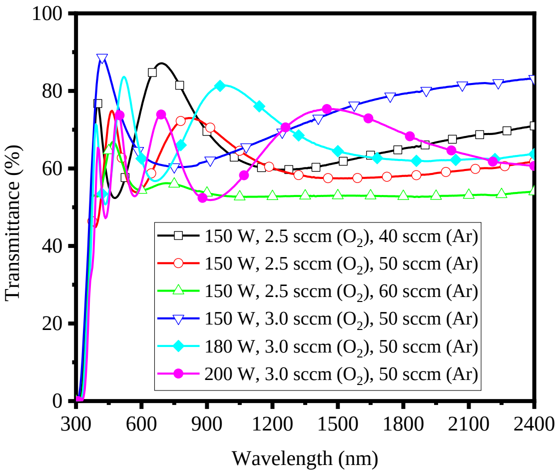

Figure 2: Spectral transmittance of Ag-doped TiO_2 films deposited at different Ti target sputtering powers, Ar and O_2 flow rates.

Crystal Structure of the Ag-doped TiO_2 Thin Films

GIXRD measurements confirmed that the crystal structure of the Ag-doped TiO_2 depends on the deposition temperature. As shown in Figure 3, at temperatures between 300 °C and 400 °C, the samples have a dominant and intense peak oriented along (101) planes at $2\theta \sim 25.28$ corresponding to the anatase crystal structure as per PDF# 21-1272. The anatase recrystallisation of TiO_2 films at lower temperatures have also been reported in literature (Ananthakumar *et al*., 2012). On the other hand, less intense peaks; (110), (210) and (220) which correspond to the rutile crystal structure, were obtained in the same temperature range (PDF# 21-1276). Samples prepared at deposition temperature of 450 °C exhibited mixed anatase-rutile structures, with the dominant rutile peak showing relatively higher intensity compared to the peak for anatase structure. This observation suggests that at a substrate temperature of or above 450 °C, the TiO_2 anatase phase can be partially transformed into a rutile phase. However, the temperature at which pure rutile structure is achieved could not be shown in this work since our sputtering system could only reach a maximum temperature of 450 °C.

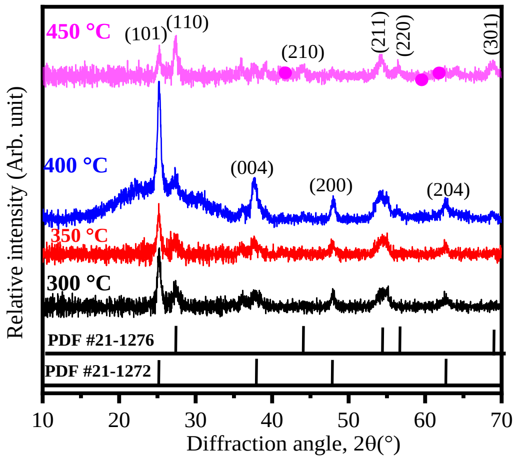

Figure 3: GIXRD spectra of Ag-doped TiO_2 thin films deposited at different substrate temperatures.

The lattice spacing (d_{hkl}) for all samples at an anatase peak aligned along (101) was calculated via Bragg's equation (Ollotu *et al*., 2020). As shown in Table 1, the values obtained correspond approximately to those of TiO_2 as per PDF# 21-1272 and there was no significant change in the values for samples prepared at different deposition temperatures.

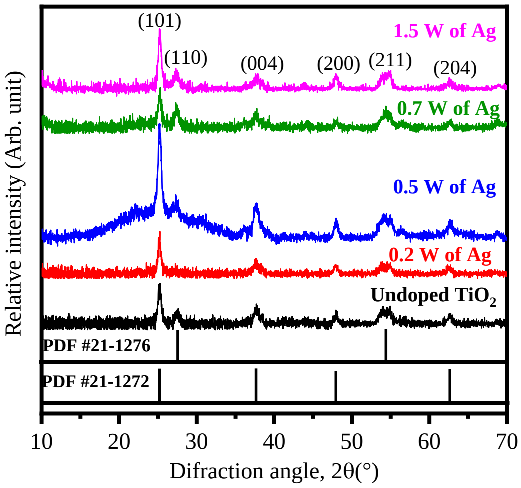

Figure 4: GIXRD spectra of the undoped and Ag-doped TiO_2 thin films.

To gain insight into the influence of substrate temperature on the crystallinity, the Full Width at Half Maximum (FWHM), β, of the dominant anatase peak oriented along the (101) plane was determined for the samples deposited at 300 °C, 350 °C, 400 °C and 450 °C, using Gaussian fitting in Origin 2018a software. The Williamson and Smallman's relation, $\varepsilon = \frac{\beta}{4\tan\theta}$, was used to compute the micro-strain (ε) of the samples and the obtained values are as presented in Table 1. The β and ε values decreased when the substrate temperature was increased from 300 °C to 350 °C, implying improvement in crystallinity. At a substrate temperature of 400 °C, both β and ε values were comparable to those of samples deposited at 350 °C. The improved crystal quality at 350 °C and 400 °C is attributed to the reduction in defects associated with crystal realignment which depends on the surface mobility of the adsorbed species. In fact, as the deposition temperature increases, the kinetic energy of the sputtered species and the mobility of adatoms also increase, thus increasing the condensation and diffusion rates of particles to form films on the substrate. Increasing the diffusion rate reduces defects and enhances the crystal quality of the films. The corresponding trend in crystal quality improvement due to increase in deposition temperature was also reported in the literature (Hasan *et al*., 2010; Yildiz *et al*. 2010).

For samples deposited at 450 °C, the crystal quality was poor, which was confirmed by the increase in β and ε with consideration of the anatase peak. This observation may be related to the transition of the crystal structure from anatase to rutile. Both rutile and anatase phases of TiO_2 have a tetragonal crystal structure, but the bond lengths between Ti-O and O-O as well as lattice parameters are not the same. Thus, the recrystallisation growth process of these two structures might not be the same as well. To compare crystal quality, the β of the rutile peak was calculated and found to be lower compared to that of anatase as shown in Table 1.

Table 1: FWHM ($\beta_{2\theta}$), micro-strain (ε) and lattice spacing (d_{hkl}) of Ag-doped TiO_2 films deposited at the different substrate temperature

Substrate temperature (°C)	2θ (degree)	$\beta_{2\theta}$ (10^{-3} radian)	ε (10^{-3} radian)	d_{hkl} (Å)
300 °C	25.22	8.87	9.91	3.528
350 °C	25.19	8.60	9.63	3.533
400 °C	25.22	8.64	9.65	3.528
450 °C (Anatase)	25.25	9.34	10.43	3.524
450 °C (Rutile)	27.38	8.10	8.31	3.254

At a deposition temperature of 400 ℃, the amount of Ag in the TiO_2 films was varied by varying the Ag target sputtering power from 0 to 1.5 W and their influence on the crystallinity of the films was investigated using GIXRD. Figure 4 shows that both undoped and doped TiO_2 films have anatase crystal structure with intense peak oriented along the (101) planes as referenced in PDF# 21-1276. There is no peak in the spectra exhibiting Ag or the corresponding oxide phases.

It was found that increasing the sputtering power shifts the peak position toward a higher diffraction angle by 0.003° at 0.5 W to 0.03° at 1.5 W from that of the undoped TiO_2 films. The shift in the diffraction angle is attributed to the slightly higher atomic mass of Ag compared to that of Ti elements. The Ag doping improves the crystallinity of the TiO_2 thin films as evidenced by the decrease in β and ε when the sputtering power was increased from 0.2 W to 1.5 W as presented in Table 2. Furthermore, insignificant variation of the lattice spacing of the doped films with varied Ag target sputtering powers was observed, implying that Ag doping may result in less lattice distortion in the TiO_2 matrix.

Table 2: FWHM ($\beta_{2\theta}$), micro-strain (ε) and lattice spacing (d_{hkl}) of Ag-doped TiO_2 films with different Ag target sputtering powers

Ag target sputtering Power (W)	2θ (degree)	$\beta_{2\theta}$ (10^{-3} radian)	ε (10^{-3} radian)	d_{hkl} (Å)
Pure TiO_2	25.22	8.79	9.82	3.528
0.2 W	25.21	8.71	9.73	3.529
0.5 W	25.22	8.64	9.65	3.528
0.7 W	25.23	8.51	9.51	3.526
1.5 W	25.24	8.51	9.51	3.525

Figure 5 shows Raman spectra of Ag-doped TiO_2 thin films deposited at different substrate temperatures. The spectra show a dominant anatase peak at 144 cm^{-1} Raman shift and less intense rutile peaks at 247 cm^{-1} and 445 cm^{-1} for samples deposited at 400 ℃. The similar peaks corresponding to anatase phases have been reported by other studies (Tuschel, 2019; El-Deen *et al.*, 2018). For samples deposited at 450 ℃, an extra peak at 610 cm^{-1} representing rutile structure was obtained, reflecting the structural transition from anatase to rutile in consistency with GIXRD results. For the different Ag sputtering powers at 400 ℃ deposition temperature, all samples showed the same anatase peaks and less intense rutile peaks as shown in Figure 6. These results show that the substrate temperature can change TiO_2 structure from anatase to rutile, but a controlled amount of Ag dopant does not change the structure as was also shown by the GIXRD measurements of Figures 3 and 4.

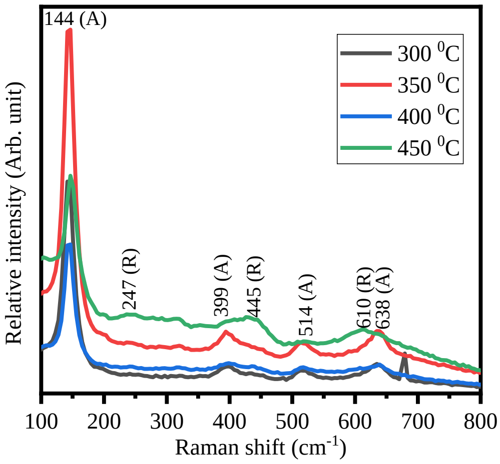

Figure 5: Raman spectra of the Ag-doped TiO_2 thin films deposited at different substrate temperatures.

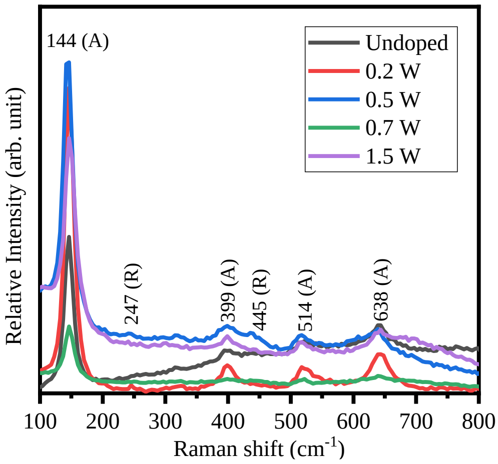

Figure 6: Raman spectra of the undoped and Ag-doped TiO_2 thin films.

Surface Morphologies of the Ag-doped TiO_2 Thin Films

Figure 7 shows SEM images of the Ag-doped TiO_2 thin films deposited at different substrate temperatures. Based on the SEM images, it was confirmed that the films were free of voids and crakes regardless of deposition temperature. Furthermore, it was observed that grain distribution, size and densification were strongly influenced by deposition temperature. At deposition temperature of 300 ℃, small spherical grains and partially agglomerated grains were observed as shown in Figure 7 (a). As the temperature was increased to 350 ℃, the small spherical grains were agglomerated and formed large grains and dense films (Figure 7 (b)). The higher density of the films at 350 ℃ is ascribed to the higher kinetic energy of the sputtered species, which increases the diffusion rate of the adatoms at the substrate. At 400 ℃ the film's surface becomes uniform and compact with large columnar grains. A further increase in deposition temperature to 450 ℃ led to recrystallisation of the films with more homogeneous grains in size and shape.

It was also observed by GIXRD analysis that samples deposited at 450 ℃ have mixed anatase and rutile structures, with rutile dominating. This could be one of the reasons for high temperature recrystallisation, since the two structures have different constituent atomic bond lengths. The randomly sized and distributed cluster of small grains in the film can increase carrier scattering and photon absorption along the boundaries, thus affecting both carrier mobility and optical transmittance.

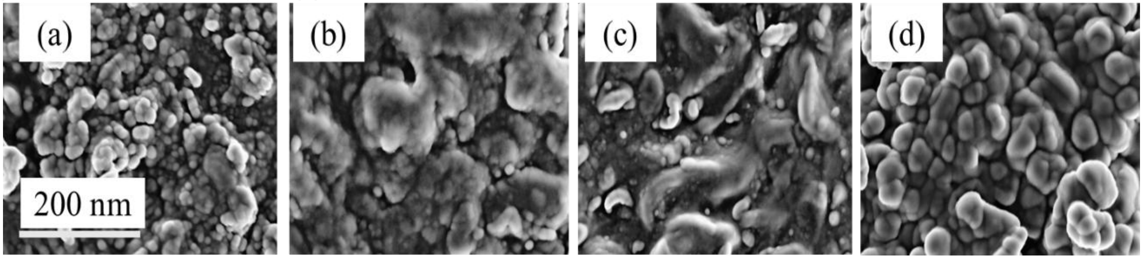

Figure 7: SEM images of Ag-doped TiO_2 films deposited at 300 ℃ (a), 350 ℃ (b), 400 ℃ (c), and 450 ℃ (d).

From AFM measurements, it was observed that the topological surface properties of the Ag-doped TiO_2 thin films were varied with increasing deposition temperature as shown in Figure 8. The films were observed to have spherical grains of different sizes and distribution. Surface roughness as one of the factors that affect the carrier mobility and light scattering and hence electrical conductivity and film transmittance was determined. It was noted that average surface roughness and root mean square (RMS) were decreasing from 6.62 nm and 8.09 nm for Ag-doped TiO_2 samples deposited at 300 ℃ to 3.47 nm and 4.41 nm for the ones deposited at 400 ℃ and then slightly increased to 4.12 nm and 4.51 nm for the ones deposited at 450 ℃, t respectively. In addition, low value of average surface roughness at 400 ℃ indicates better homogeneity and smoothness. This observation is consistent with the SEM image shown in Figure 7 (c). In general, the decrease in film roughness is attributed to the increased rate of the particles' nucleation on the substrates as temperature was increased. Furthermore, samples deposited at 300 °C and 350 °C had more voids and less dense parked grains compared to the ones deposited at 400 °C.

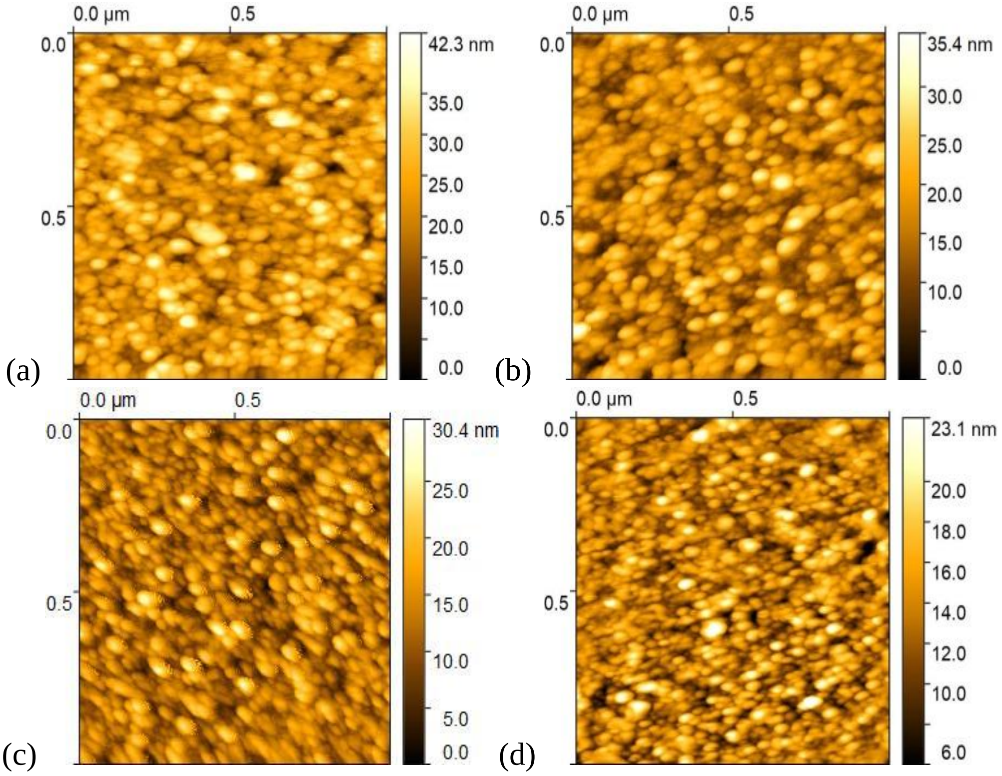

Figure 8: 2D AFM images of the Ag-doped TiO_2 thin films deposited at different substrate temperatures; (a) 300 °C (b) 350 °C (c) 400 °C, and (d) 450 °C.

Depth Profiling and Dopant's Concentration of the Ag-doped TiO_2 Thin Films

Since Ag-doped TiO_2 thin films were deposited via reactive co-sputtering, it is important to determine as to what extent the Ag atoms have diffused into the TiO_2 films. GDOES was used to determine the depth profiles of the constituent's elements (Ag, Ti and O) as shown in Figure 9. It was observed that the signal strength of the O and Ag atoms were decreasing from film's surface toward the glass surface while that of the Ti atoms was increasing in the first 20 seconds of measurements, thereafter the signal strength for all atoms were nearly constant. It can be assumed that the relative increase in the oxygen signal strength on the surface is due to atmospheric oxidation that happens just after taking out samples from the sputtering chamber. However, the reason behind the higher Ag signal strength at the film's surface is not clear. Furthermore, as the Ag target sputtering power was increased from 0.2 W to 1.5 W, the relative intensity of Ag atoms was increased while that of Ti atoms was decreased. This trend indicates that more Ti atoms are replaced by Ag atoms in the TiO_2 lattice with increasing Ag target sputtering power.

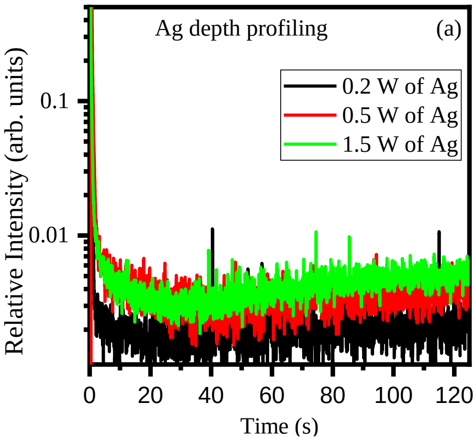

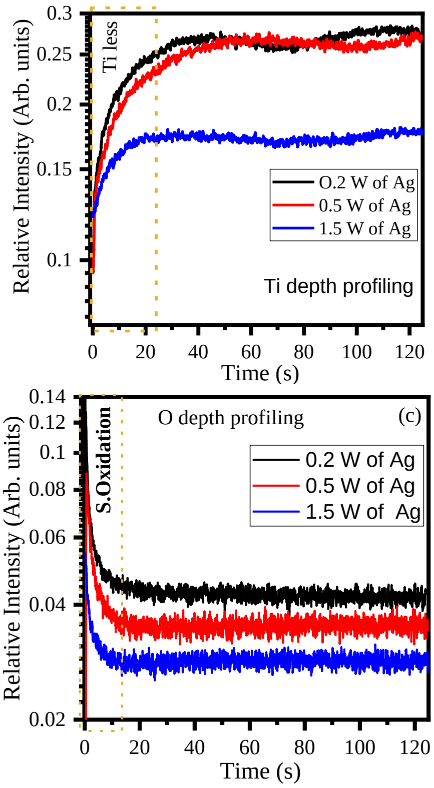

Figure 9: GDOES depth profiling of the (a) Ag, (b) Ti and (c) O atoms in Ag-doped TiO_2 through reactive co-sputtering technique.

Figure 10 shows experimental and simulated RBS spectra of the undoped and Ag-doped TiO_2 thin films at different sputtering powers to the Ag target. From the spectra, the presence of Ti, O and Ag atoms was confirmed and Si peak which originates from the glass substrate was observed. The intensity of the peaks for Ag atoms was observed to increase as the Ag target sputtering powers was increased. The atomic composition ratios of the films as determined through SIMNRA simulations are presented in Table 3. It is noted that, oxygen concentrations are lower for the doped films compared to the undoped ones, suggesting the increased oxygen vacancy in the film with Ag doping. This observation agrees with the ones from the GDOES depth profiling where O signal strength was decreasing as the Ag target sputtering power was increased.

Table 3: Atomic composition ratio of the Ag-doped TiO_2 thin films

Atoms/	Compositions at different sputtering powers of Ag			
	Pure	0.2 W	0.5 W	1.5 W
O (%)	80.72	77.58	76.56	77.1
Ti (%)	19.28	22.22	23.16	22.25
Ag (%)	0	0.20	0.28	0.61

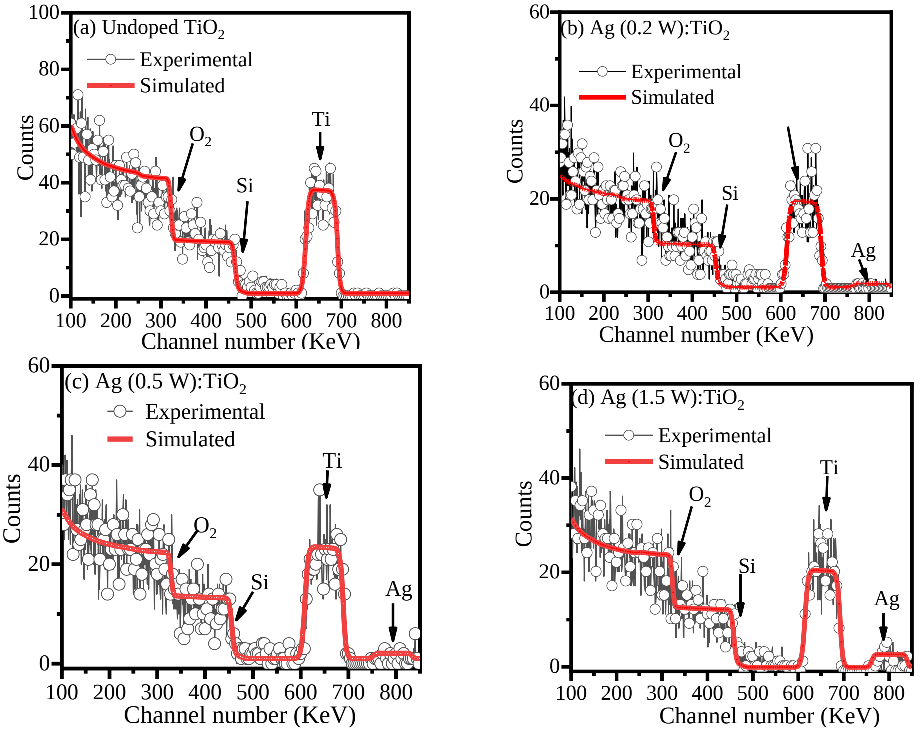

Figure 10: RBS and simulated spectra of the (a) undopedTiO_2 and doped TiO_2 with Ag at a Ag target sputtering power of (b) 0.2 W, (c) 0.5 W and (d) 1.5 W.

Optical Transmittance and Bandgap Energies of the Ag-doped TiO_2 Thin Films

Figure 11 shows the spectral transmittances of the Ag-doped TiO_2 thin films deposited at different substrate temperatures. In the wavelength range between 900 nm and 1500 nm, the transmittance increased for all samples and maximum value of about 80% was achieved for samples deposited at 300 °C and 350 °C while at 400 °C transmittance was about 75%. In the region around 500 nm, all samples had higher transmittances compared to other regions and particularly samples deposited at 350 °C and 400 °C had transmittances of approximately 80% while ones deposited at 300 °C had a transmittance of about 85%. However, the transmittance was found to slightly decrease with increase in deposition temperature.

For comparison, the weighted average of solar transmittance, T_{sol}, was calculated from the spectral transmittance and air mass 1.5 solar irradiance, G(ʎ), data using Equation 1 as described in (Tibaijuka *et al*., 2022). It was found that the average transmittance of the samples decreased from 66% to 57% when the substrate temperature was increased from 300 °C to 450 °C as shown in Figure 11 insert. The decrease in transmittance is attributed to the increase in grain size as observed from SEM images shown in Figure 7. The lower transmittance for the samples deposited at 450 °C compared to ones deposited at 400 °C could be linked to the slight increase of the average roughness as determined from the AFM images in Figure 8. Surface roughness leads to surface scattering, which enhances absorption and reduces transmittance.

$$T_{sol} = \frac{\sum_{300}^{2400} G(\lambda)T(\lambda)}{\sum_{300}^{2400} G(\lambda)} \qquad (1)$$

From the transmittance data, the absorption coefficient, α, was calculated using Equation 2 and was used to estimate the bandgap energy (E_g) of the films using the Tauc plot of $(ahv)^2$ against photon energy (hv) as per Equation 3. The bandgap was obtained by linear extrapolation of the straight part of the curve onto the horizontal axis where $(ahv)^2=0$ (Figure 12 (a)). The obtained bandgap energies for all samples ranged between 3.0 eV to 3.13 eV which is in line with values reported in the literature (El Mesoudy *et al.* 2023; Landi *et al.* 2022).

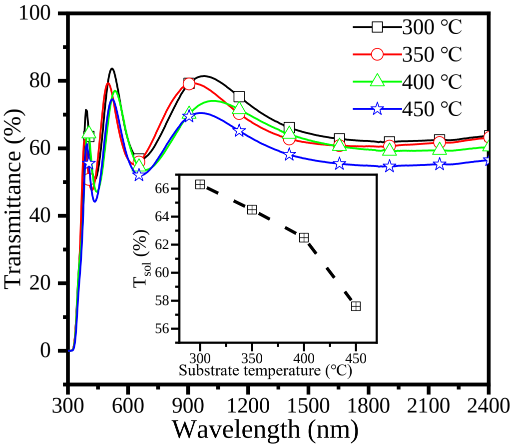

Figure 11: Spectral transmittance of the Ag-doped TiO_2 films deposited at different substrate temperatures.

Insert in the Figure shows relationship between solar average transmittance and substrate temperature. The slightly lower bandgap for samples deposited at higher temperatures might be correlated with the slight increase of the film thickness as shown in Table 4.

$$\alpha = \frac{1}{t} ln\left(\frac{1}{T}\right) \qquad (2)$$

$$(\alpha h v)^{1/2} = B\left(hv - E_g\right) \qquad (3)$$

where t is the film thickness and B is constant.

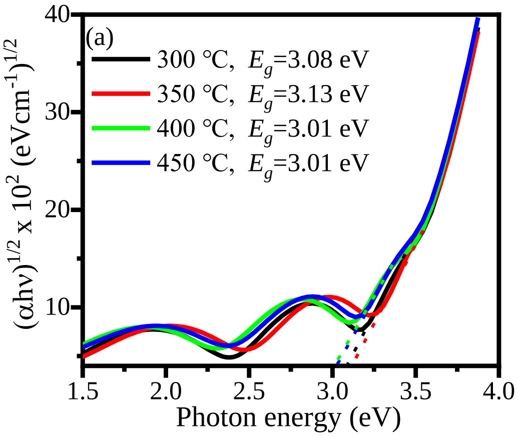

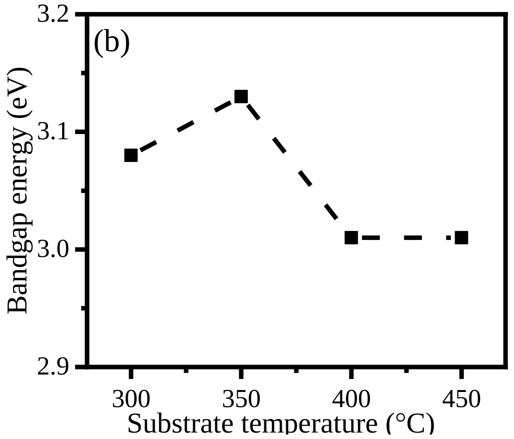

Figure 12: (a) Tauc plots and (b) bandgap energy of the Ag-doped TiO_2 films deposited at different substrate temperatures.

As shown in Figure 13 (a), the spectral transmittance of the Ag-doped TiO_2 films decreased with increasing Ag target sputtering power. The weighted average solar transmittance of the films as calculated using Equation 1, decreased from 67.4% at 0.2 W to 59.9% at 1.5 W Ag target sputtering power as shown in Table 4. The decrease in transmittance for these samples may be related to the increased amount of Ag, which is one of the highly reflective metals. The increase of the incorporated Ag amount in the TiO_2 lattice is evidenced by the GDOES and RBS measurements shown in Figures 9 and 10, respectively. It was also observed that Ag doping decreased bandgap of the films from 3.27 eV for the undoped to about 3.0 eV for the doped TiO_2 samples as shown in Figure 13 (b) and Table 4.

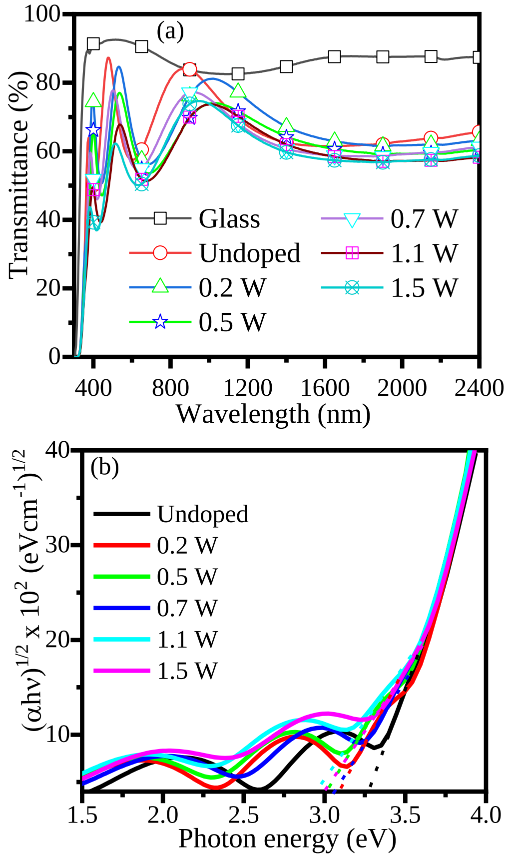

Figure 13: (a) Transmittance spectra of the undoped and Ag-doped TiO_2 films (b) Tauc plot for Ag-doped TiO_2 films.

Table 4: Weighted average solar transmittances and bandgap energies of the Ag-doped TiO_2 films

Sputtering power of Ag target (W)	0	0.2	0.5	0.7	1.1	1.5
Average solar transmittance (%)	67.36	67.42	63.34	63.29	60.58	59.96
Bandgap energy (eV)	3.27	3.1	3.01	3.06	2.96	3.00

Hall Effect Parameters of the Ag-doped TiO_2 Films

Table 5 shows the variation in electrical resistivity, carrier concentration and mobility of the Ag-doped TiO_2 films as deposition temperature was increased from 300 °C to 450 °C. The carrier concentration was found to increase from 9.55×10^{18} cm^{-3} for samples deposited at 300 °C to 1.13×10^{20} cm^{-3} for the ones deposited at 450 °C which is correlated to improvement in grain size as revealed through SEM measurements. The carrier mobility decreased from 26.69×10^{-2} $cm^2V^{-1}S^{-1}$ at 300 °C to 14.14×10^{-2} $cm^2V^{-1}S^{-1}$ at 450 °C deposition temperature, while the electrical conductivity was increased with increase in deposition temperature from 0.41 Ω^{-1} cm^{-1} to 2.56 Ω^{-1} cm^{-1} for samples deposited at

300 °C to 450 °C as shown in Figure 14. A similar trend of increasing electrical conductivity with an increase in substrate temperature was reported by Yildiz *et al.* (2010). The decrease in carrier mobility may be associated with the increase of ionized impurity scattering as a result of increased carrier concentration.

Table 5: Thickness, carrier concentration, carrier mobility and conductivity of Ag-doped TiO_2 films

Temperature (°C)	Thickness (nm)	Carrier Concentration × 10^{19} (cm^{-3})	Carrier Mobility × 10^{-2} ($cm^2V^{-1}S^{-1}$)	Conductivity (Ωcm)$^{-1}$
300	180	0.955	26.69	0.41
350	190	1.835	19.1	0.56
400	196	5.277	15. 27	1.34
450	206	11.28	14.14	2.56

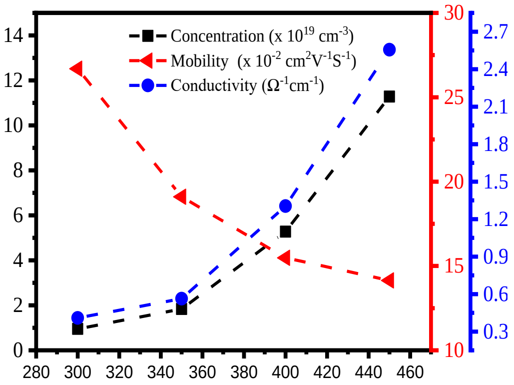

Figure 14: Carrier concentration, mobility, and electrical conductivity of the Ag-doped TiO_2 films deposited at different substrate temperature.

As to the effect of Ag doping on TiO_2 hall parameters, all the doped samples had higher conductivity and carrier concentration compared to the undoped ones as presented in Table 6. The improved conductivity for doped samples is connected to the incorporated Ag atoms in the matrix of TiO_2. However, when the dopant's target sputtering power was increased further from 0.2 W to 1.5 W, corresponding to Ag concentration of 0.2% and 0.61%, respectively, the electrical conductivity decreased from 2.05 $\Omega^{-1}cm^{-1}$ to 1.12 $\Omega^{-1}cm^{-1}$, respectively. It was observed that Ag doping increases the carrier concentration of TiO_2 thin films by one order of magnitude compared to undoped samples, although no clear trend was noted for the carrier concentration and mobility as the Ag concentration in the samples was increased.

Table 6: Hall effect parameters of the Ag-doped TiO_2 films with different Ag target sputtering powers

Ag target Sputtering power (W)	Carrier concentration (10^{19} cm^{-3})	Carrier Mobility (10^{-1} $cm^2V^{-1}S^{-1}$)	Conductivity (Ωcm)$^{-1}$
0	0.45	10.32	0. 74
0.2	3.29	3.89	2.05
0.5	5.28	1.53	1.34
0.7	1.22	6.89	1.34
1.1	1.72	4.34	1.20
1.5	3.74	1.87	1.12

CONCLUSION AND RECOMMENDATION

In this study, the influence of substrate temperature and Ag doping concentration on the properties of Ag-doped TiO_2 thin films deposited by co-sputtering of Ti and Ag targets under controlled O_2 and Ar gas flow rates was investigated. It was found that the electrical conductivity increased from 0.41 $\Omega^{-1}cm^{-1}$ to 2.56 $\Omega^{-1}cm^{-1}$ and the average solar transmittance decreased from 66% to 57% as the substrate temperature was increased from 300 °C to 450 °C. The bandgap of Ag-doped TiO_2 samples deposited at different substrate temperatures was found to range from 3.0 eV to 3.13 eV. Undoped samples had higher bandgap energies compared to those of doped ones, though there was no significant change observed in the bandgap for different Ag doping levels. Taking into account both transmittance and conductivity, the samples with Ag and Ti concentrations of 0.28% and 23.16%, respectively, confirmed via RBS analysis, deposited at 400 °C exhibited both higher electrical conductivity and transmittance. In addition, SEM revealed that these samples had a large grain size and uniformly compacted films compared to other samples. Therefore, the results of this study explore the potential deposition approach for Ag-doped TiO_2 thin films for various applications including as transparent conducting oxide in photo-electronic devices. However, to realise the practical applications for Ag-doped TiO_2 as a transparent conducting oxide in photo-electronic devices, particularly solar cells, there is a need to fabricate solar cells with it and investigate the device's performance. Furthermore, it is interesting to gain insight on the quality of the interface between the Ag-doped TiO_2 transparent contact and other solar cell's layers and hence device performance.

ACKNOWLEDGEMENTS

Authors present special thanks to the International Science Programme (ISP) for research equipment and materials, and for the three months fellowship for HBS. HBS acknowledges the University of Dar es Salaam for Ph.D. scholarship. The Division of Solar Cell Technology, Uppsala University and Prof. Charlotte Platzer-Björkman are acknowledged for hosting HBS in their laboratory and providing access to research facilities. Jan Keller, Comparotto Corrado and Aggarwal Garima are acknowledged for their help in the characterisation of samples with GDOES, RBS and GIXRD techniques, respectively.

REFERENCES

Agirseven O., Rivella D.T., Haggerty J.E.S., Berry P.O., Diffendaffer K., Patterson A., Kreb J., Mangum J.S., Gorman B.P., Perkins J.D., Chen B.R., Schelhas L. T. and Tate J. (2020). Crystallization of TiO_2 polymorphs from RF-sputtered, amorphous thin-film precursors. *AIP Advances*, **10**(2): 025109. doi.:10.1063/1.5140368

Al-Maliki F.J., Hammadi O.A., Chiad B.T. and Al-Oubidy E.A. (2020). Photocatalytic activity of Ag-doped TiO_2 nanostructures synthesized by DC reactive magnetron co-sputtering technique. *Optical and Quantum Electronics*, **52**: 1-9. doi.:10.1007/s11082-020-02315-7

Ananthakumar R., Subramanian B., Yugeswaran S. and Jayachandran M. (2012). Effect of substrate temperature on structural, morphological and optical properties of crystalline titanium dioxide films prepared by DC reactive magnetron sputtering. *Journal of Materials Science: Materials in Electronics*, **23**: 1898-1904. doi.:10.1007/s10854-012-0681-1

Chakhtouna H., Benzeid H., Zari N., Qaiss A. E. K. and Bouhfid R. (2021). Recent progress on Ag/TiO_2 photocatalysts: Photocatalytic and bactericidal behaviors. *Environmental Science and Pollution Research*, **28**: 44638-44666. doi.:10.1007/s11356-021-14996-y

Chihi A., Boujmil M.F. and Bessais B. (2017). Investigation on the performance of CIGS/TiO_2 heterojunction using SCAPS software for highly efficient solar cells. *Journal of Electronic Materials*, **46**: 5270-5277. doi.:10.1007/s11664-017-5547-0

Das N.K., Chakrabartty J., Farhad S.F.U., Gupta A.S., Ahamed E.I., Rahman K.S., Wafi A., Alkahtani A.A., Matin M.A. and Amin N. (2020). Effect of substrate temperature on the properties of RF sputtered CdS thin films for solar cell applications. *Results in Physics*, **17**:

103132. doi.:10.1016/j.rinp.2020.103132

El-Deen S.S., Hashem A.M., Abdel Ghany A. E., Indris S., Ehrenberg H., Mauger A. and Julien C. M. (2018). Anatase TiO_2 nanoparticles for lithium-ion batteries. *Ionics*, **24**: 2925-2934. doi.:10.1007/s11581-017-2425-y

El Mesoudy A., Machon D., Ruediger A., Jaouad A., Alibart F., Ecoffey S. and Drouin D. (2023). Band gap narrowing induced by oxygen vacancies in reactively sputtered TiO_2 thin films. *Thin Solid Films*, **769**:139737. doi.:10.1016/j.tsf.2023.139737

Ellmer K. (2012). Past achievements and future challenges in the development of optically transparent electrodes. Nature *Photonics*, **6**(12): 809-817. doi.:10.1038/nphoton.2012.282

Granqvist C.G. (2007). Transparent conductors as solar energy materials: A panoramic review. Sol. *Solar Energy Materials and Solar Cells*, **91**(17): 1529-1598. doi.:10.1016/j.solmat.2007.04.031

Green M.A. (2009). Estimates of Te and In prices from direct mining of known ores. *Progress in Photovoltaics: Research and Applications*, **17**(5): 347-359. doi.:10.1002/pip.899

Haji H.F., Numan N., Madiba I.G., Mabakachaba B., Mtshali C., Khumalo Z. Kotsedi L., Mlyuka N.R., Samiji M.E. and Maaza M. (2023). Zn and W co-doped VO_2-based thin films prepared by dc magnetron sputtering: improved luminous transmittance and reduced transition temperature. *Journal of Electronic Materials*, **52**: 1-10. doi.:10.1007/s11664-023-10382-1

Hasan M.M., Haseeb A.S.M.A., Saidur R., Masjuki H.H. and Hamdi M. (2010). Influence of substrate and annealing temperatures on optical properties of RF-sputtered TiO_2 thin films. *Optical Materials*, **32**(6): 690-695. doi.:10.1016/j.optmat.2009.07.011

Horcas I., Fernández R., Gomez-Rodriguez J. M., Colchero J.W.S.X., Gómez-Herrero J.W.S.X.M. and Baro A.M. (2007). WSXM: A software for scanning probe microscopy and a tool for nanotechnology. *Review of scientific instruments*, **78**(1): 013705. doi.:10.1063/1.2432410

Ifeoma A. and Jude O. (2018). Analysis of pure and Ag-doped TiO_2 thin films deposited by field assisted spray pyrolysis. *Chemical Science International Journal*, **24**(4): 1-10. doi.:10.9734/CSJI/2018/43904

Landi J.S., Segundo I.R., Afonso C., Lima J.O., Costa M.F., Freitas E., Carneiro J. (2022). Evaluation of band gap energy of TiO_2 precipitated from titanium sulphate. *Physica B: Condensed Matter*, **639**:414008. doi.:10.1016/j.physb.2022.414008

Lei X.F., Xue X.X. and Yang H. (2014). Preparation and characterization of Ag-doped TiO_2 nanomaterials and their photocatalytic reduction of Cr (VI) under visible light. *Applied Surface Science*, **321**: 396-403. doi.:10.1016/j.apsusc.2014.10.045

Liaqat M.A., Hussain Z., Khan Z., Akram M.A. and Shuja A. (2020). Effects of Ag doping on compact TiO_2 thin films synthesized via one-step sol–gel route and deposited by spin coating technique. *Journal of Materials Science: Materials in Electronics*, **31**: 7172-7181. doi.:10.1007/s10854-020-03288-9

Lu Z., Jiang X., Zhou B., Wu X. and Lu L. (2011). Study of effect annealing temperature on the structure, morphology and photocatalytic activity of Si doped TiO_2 thin films deposited by electron beam evaporation. *Applied Surface Science*, **257**(24): 10715-10720. doi.:10.1016/j.apsusc.2011.07.085

Mlyuka N.R. and Kivaisi R.T. (2006). Correlation between optical, electrical and structural properties of vanadium dioxide thin films. *Journal of Materials Science*, **41**:5619–5624. doi.:10.1007/s10853-006-0261-y

Mlyuka N.R., Niklasson G.A. and Granqvist C.G. (2009). Thermochromic multilayer films of VO_2 and TiO_2 with enhanced transmittance. *Solar Energy Materials and Solar Cells*, **93**(9): 1685-1687. doi.:10.1016/j.solmat.2009.03.021

Mwakyusa L.P., Mlyuka N.R. and Samiji M.E. (2022). Boron doped ZnO films deposited by DC Reactive sputtering using Zn: B Target: Influence of the deposition temperature on the structural, electrical and optical properties.

Tanzania Journal of Science, **48**(1), 148-155. doi.:10.4314/tjs.v48i1.14

Naghdi S., Rhee K.Y., Hui D. and Park S.J. (2018). A review of conductive metal nanomaterials as conductive, transparent, and flexible coatings, thin films, and conductive fillers: Different deposition methods and applications. *Coatings*, **8**(8): 278. doi.:10.3390/coatings8080278

Nečas D. and Klapetek P. (2012). Gwyddion: an open-source software for SPM data analysis. *Open Physics*, **10**(1): 181-188. doi.:10.2478/s11534-011-0096-2

Nisika N., Kaur K., Yadav, M.K., Bag A. and Kumar M. (2021). Suppression of interfacial oxygen vacancies for efficient charge extraction at CZTS/TiO$_2$ heterojunction. *Applied Physics Letters*, **118**(4): 041601. doi.:10.1063/5.0038458

Ollotu E.R., Nyarige J.S., Mlyuka N.R., Samiji M.E. and Diale M. (2020). Properties of ITO thin films rapid thermally annealed in different exposures of nitrogen gas. *Journal of Materials Science: Materials in Electronics*, **31**:16406-16413. doi.:10.1007/s10854-020-04192-y

Panigrahi M.R. and Devi M. (2019). Variation of optical and electrical properties of Zr doped TiO$_2$ thin films with different annealing temperatures. *Journal of Physics: Conference Series*, **1172**(1): 012046. doi.:10.1088/1742-6596/1172/1/012046

Peng J., Duong T., Zhou X., Shen H., Wu Y., Mulmudi H.K., Wan Y., Zhong D., Li J., Tsuzuki T., Weber K.J., Catchpole K.R. and White T.P. (2017). Efficient indium-doped TiO$_x$ electron transport layers for high-performance perovskite solar cells and perovskite-silicon tandems. *Advanced Energy Materials*, **7**(4): 1601768. doi.:10.1002/aenm.201601768

Platzer-Björkman C., Barreau N., Bär M., Choubrac L., Grenet L., Heo J., Kubart T., Mittiga A., Sanchez Y., Scragg J., Sinha S. and Valentini M. (2019). Back and front contacts in kesterite solar cells: State-of-the-art and open questions. *Journal of Physics: Energy*, **1**(4): 044005. doi.:10.1088/2515-7655/ab3708

Roose B., Pathak S. and Steiner U. (2015). Doping of TiO$_2$ for sensitized solar cells. *Chemical Society Reviews*, **44**(22): 8326-8349. doi.:10.1039/C5CS00352K

Sawa H.B., Samiji M.E. and Mlyuka N.R. (2018). Effects of selenized DC sputtered precursor stacking orders on the properties of Cu$_2$ZnSnSe$_4$ absorber layer for thin film solar cells. Tanz. J. Sci., **44**(4): 1-11.

Sawa H.B. (a), Babucci M., Donzel-Gargand O., Pearson P., Hultqvist A., Keller J., Platzer-Björkman C., Samiji M.E. and Mlyuka N.R. (2024). Enhanced performance of Cu$_2$ZnSnS$_4$ based bifacial solar cells with FTO and W/FTO back contacts through absorber air annealing and Na incorporation. *Solar Energy Materials and Solar Cells*, **264**:112605. doi.:10.1016/j.solmat.2023.112605

Sawa H.B. (b), Babucci M., Keller J., Platzer Björkman C., Mlyuka N.R. and Samiji M.E. (2024). Effects of Al$_2$O$_3$ rear interface passivation on the performance of bifacial kesterite-based solar cells with Fluorine-doped tin dioxide back contact. *Physica status solidi (b)*: **261**(10): 2400080. doi.:10.1002/pssb.202400080

Shana E., Mlyuka N., Samiji M., and Sungi G. (2023). Effects of sputtering power and film thickness schemes on electrical, structural, morphology and optical properties of Mo tri-layer back contact for Kesterite thin film solar cells, *AIP Conference Proceedings*, **3040** (1):070008. doi.:10.1063/5.0175550

Shao G.N. (2024). Sol-gel synthesis and Microstructure Characterization of NiO-TiO$_2$ Semiconductor. *Tanzania Journal of Engineering and Technology*, **43**(1): 1-13. doi.:10.52339/tjet.v43i1.970.

Sheini N.A. and Rohani M. (2016). Ag-doped titanium dioxide gas sensor. In IOP Conference Series: *Materials Science and Engineering*, **108**(1):1-7. doi.:10.1088/1757-899X/108/1/012033

Soylu S.K., Atmaca İ., Asiltürk M. and Doğan A. (2019). Improving heat transfer performance of an automobile radiator using Cu and Ag-doped TiO$_2$ based nanofluids. *Applied Thermal Engineering*, **157**: 113743.

doi.:10.1016/j.applthermaleng.2019.113743

Tavakoli M.M., Yadav P., Tavakoli R. and Kong J. (2018). Surface engineering of TiO_2 ETL for highly efficient and hysteresis-less planar perovskite solar cell (21.4%) with enhanced open-circuit voltage and stability. *Advanced Energy Materials*, **8**(23): 1800794. doi.:10.1002/aenm.201800794

Tibaijuka J.J., Samiji M.E., Diale M. and Mlyuka, N.R. (2022). Effects of multilayer structure on the microstructure and optical properties of the DC sputtered chromium thin films for selective solar absorber applications. *Tanzania Journal of Science*, **48**(3): 660-667. doi.:10.4314/tjs.v48i3.13

Tuschel D. (2019). Raman spectroscopy and polymorphism. *Spectroscopy*, 34(3): 10-21.

Wu M.C., Chan S.H., Jao M.H. and Su W.F. (2016). Enhanced short-circuit current density of perovskite solar cells using Zn-doped TiO_2 as electron transport layer. *Solar Energy Materials and Solar Cells*, **157**: 447-453. doi.:10.1016/j.solmat.2016.07.003

Yildiz A., Lisesivdin S.B., Kasap M.E.H.M.E.T. and Mardare D. (2010). The substrate temperature dependent electrical properties of titanium dioxide thin films. *Journal of Materials Science: Materials in Electronics*, **21**: 692-697. doi.:10.1007/s10854-009-9979-z

Yin G., Ma J., Jiang H., Li J., Yang D., Gao F., Zeng J., Liu Z. and Liu S.F. (2017). Enhancing efficiency and stability of perovskite solar cells through Nb-doping of TiO_2 at low temperature. *ACS Applied Materials & Interfaces*, **9**(12): 10752-10758. doi.:10.1021/acsami.7b01063

Zhang X., Wu Y., Huang Y., Zhou Z. and Shen S. (2016). Reduction of oxygen vacancy and enhanced efficiency of perovskite solar cell by doping fluorine into TiO_2. *Journal of Alloys and Compounds*, **681**: 191-196. doi.:10.1016/j.jallcom.2016.04.194

Zhang W., Hu K., Tu J., Aierken A., Xu D., Song G., Sun X., Li L., Chen K., Zhang D., Zhuang Y. (2021). Broadband graded refractive index $TiO_2/Al_2O_3/MgF_2$ multilayer antireflection coating for high efficiency multi-junction solar cell. *Solar Energy*, **217**: 271-279. doi.:10.1016/j.solener.2021.01.012.